Wei Zhang
State Key Laboratory of Structural Analysis for Industrial Equipment, Department of Engineering Mechanics, Dalian University of Technology, Dalian 116023, China

Fan Jin
State Key Laboratory of Structural Analysis for Industrial Equipment, Department of Engineering Mechanics, Dalian University of Technology, Dalian 116023, China

Sulin Zhang
Department of Engineering Science and Mechanics, Department of Materials Science and Engineering, The Pennsylvania State University, University Park, PA 16802

Xu Guo[1]
State Key Laboratory of Structural Analysis for Industrial Equipment, Department of Engineering Mechanics, Dalian University of Technology, Dalian 116023, China
e-mail: guoxu@dlut.edu.cn

Adhesive Contact on Randomly Rough Surfaces Based on the Double-Hertz Model

*A cohesive zone model for rough surface adhesion is established by combining the double-Hertz model (Greenwood, J. A., and Johnson, K. L., 1998, "An Alternative to the Maugis Model of Adhesion Between Elastic Spheres," J. Phys. D: Appl. Phys., **31**, pp. 3279–3290) and the multiple asperity contact model (Greenwood, J. A., and Williamson, J. B. P., 1966, "Contact of Nominally Flat Surfaces," Proc. R. Soc. Lond. A, **295**, pp. 300–319). The rough surface is modeled as an ensemble of noninteracting asperities with identical radius of curvature and Gaussian distributed heights. By applying the double-Hertz theory to each individual asperity of the rough surface, the total normal forces for the rough surface are derived for loading and unloading stages, respectively, and a prominent adhesion hysteresis associated with dissipation energy is revealed. A dimensionless Tabor parameter is also introduced to account for general material properties. Our analysis results show that both the total pull-off force and the energy dissipation due to adhesive hysteresis are influenced by the surface roughness only through a single adhesion parameter, which measures statistically a competition between compressive and adhesive forces exerted by asperities with different heights. It is also found that smoother surfaces with a small adhesion parameter result in higher energy dissipation and pull-off force, while rougher surfaces with a large adhesion parameter lead to lower energy dissipation and pull-off force.* [DOI: 10.1115/1.4026019]

Keywords: adhesive contact, rough surface, cohesive zone model, double-Hertz theory, adhesion hysteresis

1 Introduction

It is well known that surface adhesion plays a crucial role in microscale contact problems. For smooth contact surfaces, there exist three famous theories for adhesive contact between elastic spheres proposed by Johnson et al. [1] (JKR model), Derjaguin et al. [2] (DMT model) and Maugis [3] (M-D model), respectively. In particular, a continuous transition between JKR and DMT can be achieved by the M-D model, which is applicable for more general materials with any Tabor parameter [4,5]. In parallel with the M-D model, Greenwood and Johnson [6] put forward an alternative simple and useful adhesive contact model known as the double-Hertz (D-H) model. In this model, the difference between two Hertzian pressure distributions was employed to represent the adhesive tensile stress between two contact surfaces. It was found that results obtained by the D-H model are very close to those from the M-D model. An obvious advantage of the double-Hertz model is that the analysis relies solely on the classical Hertzian solutions, which makes it more analytically tractable than the Maugis's theory. For this reason, the double-Hertz model is often favored in the studies of adhesion involving more complex contact systems, such as contact on rough surfaces [7], viscoelastic materials [8], and functionally graded elastic materials [9].

In fact, even a highly polished surface may have surface roughness on multiple length scales. Modeling the contact mechanics between rough surfaces with adhesion, however, is a challenging task. Several theoretical approaches have been developed to account for the mechanics of contact involving surface roughness. In a seminal paper, Greenwood and Williamson [10] modeled rough surfaces as an ensemble of noninteracting asperities with identical radius of curvature and height which follows a Gaussian distribution. In this model, the classical Hertz theory was applied to the contact analysis of each individual asperity. Following this idea, Fuller and Tabor [11] investigated the adhesive contact between rough surfaces by utilizing the JKR theory to study the contact of each individual asperity. They found that the adhesion behavior solely depends on a single parameter, i.e., the ratio between the dispersion of asperity heights and the maximum elastic extension which an asperity can sustain before the contact pair breaks apart. This parameter represents the statistical average of a competition between the compressive forces exerted by the higher asperities and the adhesive forces of the lower asperities. A similar model was then proposed by Maugis [12] who adopted the DMT model to analyze the contact of each individual asperity. Generally speaking, the JKR-based rough contact model is more suitable for describing the contact between relatively large and soft bodies, while the DMT-based rough contact model is more suitable for contact problems between small and rigid bodies. To bridges the gap between the solutions of these two models, Morrow et al. [13] developed a cohesive zone model for rough surfaces by applying the M-D theory to each asperity of rough surfaces. Since the adhesive traction outside the contact zone was included in each contact asperity, a transition between JKR-based and DMT-based rough contact solution was captured. A common conclusion in the above multiple asperity contact models is that increasing roughness may result in a monotonic decrease of adhesion. This result was later validated by experiments for large surface roughness, where the interaction between asperities can be ignored [14,15]. Recently, the multiple asperity contact models were extended to account for power-law shaped rough asperities [16], interactions between asperities [17–19], non-Gaussian surface roughness [20], and a fretting contact case [21]. Moreover, several theoretical methods have also been proposed to examine the adhesive behaviors of various rough surfaces, such as the self-affine fractal surface [7,22], periodic surface roughness [23], and sinusoidal undulations [24–29].

[1]Corresponding author.
Manuscript received October 15, 2013; final manuscript received November 10, 2013; accepted manuscript posted November 14, 2013; published online December 12, 2013. Editor: Yonggang Huang.

On the other hand, adhesion hysteresis was found to be a common phenomenon in adhesive contact of rough surfaces, where the work needed to separate two surfaces is usually greater than that gained by adjoining them together. Under this circumstance, the measured curve is widely observed to show two distinct branches associated with the loading and unloading stages, respectively. The area of the hysteresis loop formed by the loading and unloading branches quantifies the value of energy dissipation [30–32]. Kesari et al. [15] reported an experiment result and revealed that adhesion hysteresis may exist without moisture, plasticity, and viscoelasticity, but only depends on adhesion and roughness. To interpret this result theoretically, Kesari and Lew [33] developed a JKR-type adhesion solution to capture the effective macroscopic adhesive contact behavior of small rough surface, which agrees well with the experiment data. Later on, the case in which power-law graded solids are involved has also been studied [34]. For larger roughness sizes, the roughness-adhesion mechanism was also revealed in the multiple asperity contact model [35]. Based on the JKR-based rough contact model [11], Wei et al. [35] investigated the effect of roughness on adhesion hysteresis and provided equations for measuring the contact forces in the loading and unloading phases. The resulting energy loss was found to depend on a dimensionless parameter which is the same as the adhesion parameter in the Fuller and Tabor model [11]. Up to now, it remains a challenge to characterize the adhesion hysteresis on rough surfaces with use of a cohesive zone model, which is available for various materials with different Tabor parameters.

The main purpose of the present paper is to develop an adhesive contact model of rough surfaces which is applicable to the full range of Tabor parameters. The distinct feature of our work is that the double-Hertz model is employed to describe the contact behavior of each asperity. With use of the proposed model, not only the adhesive forces exerted by the asperities in intimate contact are considered, the effect of noncontact asperities within the range of adhesive interaction is also accounted for appropriately. Special emphasis is also placed on investigating the effects of surface roughness on the total pull-off force and energy dissipation due to adhesion hysteresis. The remainder of the paper is organized as follows. First, the main results of the double-Hertz theory for a single contact asperity are summarized in Sec. 2. The established equilibrium equations in Sec. 2 are then expressed in a curve-fitted explicit form in Sec. 3. The rough contact model is established and the corresponding solution for the total applied force is derived in Sec. 4. Based on these results, the adhesion hysteresis and the total pull-off force of the rough contact system are examined systematically in Sec. 5. Some concluding remarks are finally provided in Sec. 6.

2 Double-Hertz Solution for a Single Contact Asperity

In this section, we shall first study the single asperity contact problem, which constitutes the theoretical basis of the present work. Figure 1 shows an elastic sphere of radius R in adhesive contact with a rigid half-space under a normal loading P (negative when tensile). The spherical asperity has a constant Young's modulus E and a constant Poisson's ratio ν. Between the two contacting surfaces, the corresponding surface traction consists of two terms: the Hertz pressure p_H acting on a circular contact region of radius a and the adhesive tension p_A acting on an interaction zone of radius c. The annular region bounded by radii a and c is a noncontact but still interacting region known as the cohesive zone. Greenwood and Johnson [6] observed that the difference between two Hertzian pressure distributions with contact radii a and c can be used to describe p_A, and proceeded further to derive the dimensionless $P-a-c$, $\delta-a-c$ and $c-a$ relations as

$$P^* = \frac{2}{3\pi}[a^{*3} - \lambda(c^{*3} - a^{*3})] \tag{1}$$

$$\delta^* = a^{*2} - \lambda(c^{*2} - a^{*2}) \tag{2}$$

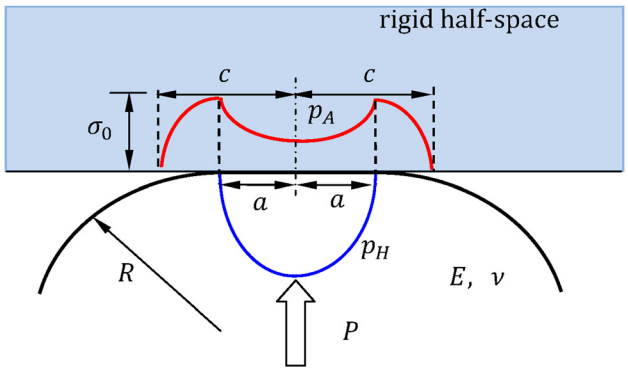

Fig. 1 Schematic illustration of an elastic spherical asperity in adhesive contact with a rigid half-space under a normal force *P* (negative when tensile). The surface traction consists of two terms: the Hertz pressure p_H acting on the contact zone of radius *a* and an adhesive traction p_A acting on the interaction zone of radius *c*, respectively.

$$1 = \lambda(1+\lambda)\frac{2}{3\pi}(c^* - a^*)^2(c^* + 2a^*) \tag{3}$$

where the nondimensional parameters in the above equations are defined as

$$a^* = \frac{a}{(R^2\Delta\gamma/E^*)^{1/3}} \tag{4}$$

$$c^* = \frac{c}{(R^2\Delta\gamma/E^*)^{1/3}} \tag{5}$$

$$P^* = \frac{P}{2\pi R\Delta\gamma} \tag{6}$$

$$\delta^* = \frac{\delta}{\bar{\delta}} = \frac{\delta}{(R\Delta\gamma^2/E^{*2})^{1/3}} \tag{7}$$

with $\Delta\gamma$ and $E^* = E/(1-\nu^2)$ denoting the surface energy and the effective elastic modulus of the elastic asperity, respectively.

By introducing the following Tabor parameter

$$\mu = \sigma_0\left(\frac{R}{E^{*2}\Delta\gamma}\right)^{1/3} \tag{8}$$

where the so-called maximum adhesive stress σ_0 is defined as

$$\sigma_0 = \lambda\frac{2E^*}{\pi R}(c^2 - a^2)^{1/2} \tag{9}$$

a relationship between λ in Eqs. (1)–(3) and the Tabor parameter can be established as

$$\mu = \lambda\frac{2}{\pi}(c^{*2} - a^{*2})^{1/2} \tag{10}$$

Up to this point, for given material properties (i.e., prescribed μ), the relations among P^*, δ^*, c^*, and a^* have been fully determined by combining Eqs. (1)–(3) and (10). As an extension, the equilibrium equations in the absence of a contact zone ($a = 0$) reduce to

$$P^* = -\frac{2}{3\pi}\lambda c^{*3} \tag{11}$$

$$\delta^* = \frac{1.5}{\mu} + \frac{1-\lambda}{2}c^{*2} \tag{12}$$

where

$$\lambda^2 = \frac{\pi^2 \mu^3}{12}(1+\lambda) \tag{13}$$

Figure 2 depicts the variations of a^* and c^* against the applied load P^* for an intermediate value of the Tabor parameter, i.e., $\mu = 1$. The noncontact extension for c^* curve is shown (dashed line) for completeness. The corresponding JKR and DMT limiting solutions are also included for comparison. It can be seen from Fig. 2 that the DMT curve can be obtained from the Hertz curve by simply shifting a value of $2\pi R\Delta\gamma$ horizontally, while the JKR curve falls between the c^* and a^* curves. As μ increases, both c^* and a^* curves are expected to collapse to the JKR curve.

Figure 3 plots the equilibrium $P-\delta$ curves for different values of the Tabor parameter. In this figure, the horizontal tangent corresponds to the normalized pull-off force P_c^*, which measures the maximum load carrying capacity of the adhesive interface. Under a displacement control condition, the vertical tangent in the $P-\delta$ curves for $\mu > 1$ represents the normalized maximum extension $\delta_c^* = \delta_c/\bar{\delta}$ at which an abrupt pull-off occurs, while for $\mu < 1$, δ_c^* corresponds to the extension at which the tensile force finally vanishes. The loading and unloading paths are distinct at zero indentation depth, which form a hysteresis loop within the regime of $\delta^* < 0$, whose area quantifies the energy dissipation during a loading/unloading cycle. Both P_c^* and δ_c^* for a single contact asperity are important factors in the following contact analysis of rough surfaces.

3 Approximation of the Double-Hertz Solution

As shown in Eqs. (1)–(3) and Eqs. (11)–(13), the double-Hertz equations provide an implicit relationship among P^*, δ^*, a^*, and c^*, which is not convenient for further analytical treatments. To circumvent this problem, in the present work, the $P^*-\delta^*$ relation is expressed in an explicit form by using the curve fitting method through a nonlinear regression process. Depending on the values of μ, the equilibrium $P^*-\delta^*$ curves are fitted numerically in the following two cases.

For $\mu \geq 1$, the equilibrium $P^*-\delta^*$ curve is fitted in a two-stage process. Firstly, the dimensionless load P^* is fitted in terms of a^* and δ^* through the following form:

$$P^* = \beta_1 + \beta_2 a^* \delta^{*b_1} + \beta_3 a^* \delta^{*b_2} \tag{14}$$

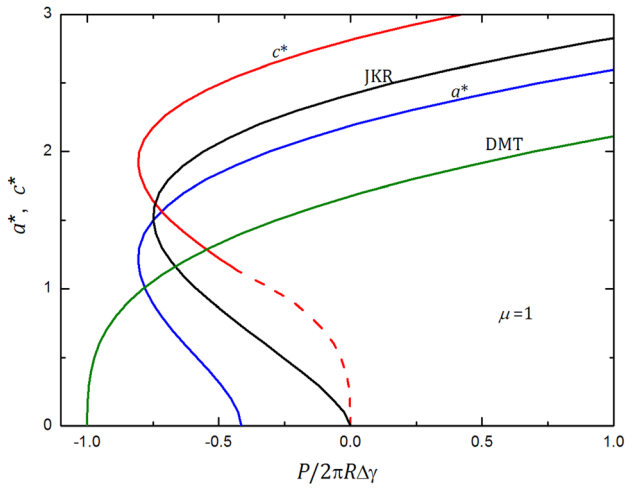

Fig. 2 The variations of a^* and c^* with respect to P^* in the double-Hertz model with $\mu = 1$. The corresponding JKR and DMT limiting solutions are also shown for comparison. The noncontact extension in the c^* curve is shown (dashed line) for completeness.

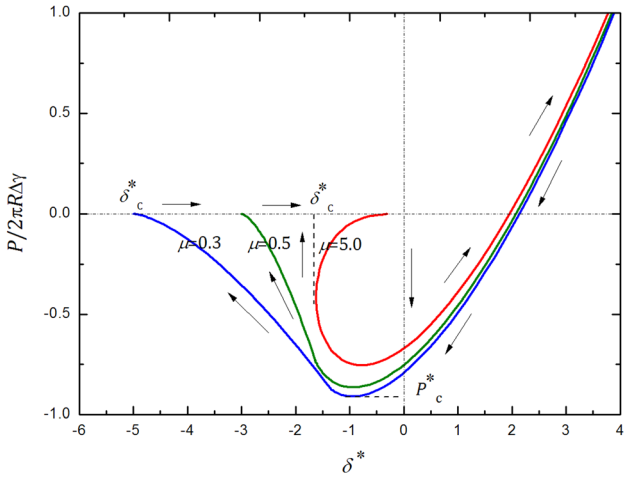

Fig. 3 The equilibrium $P-\delta$ curves in the double-Hertz model for a single contact asperity under different values of the Tabor parameter. Here P_c represents the pull-off force and δ_c corresponds to the maximum extension.

Secondly, a^* is fitted in terms of δ^* as

$$a^* = \beta_4 + (\beta_5 + \beta_6 \delta^*)^{b_3} \tag{15}$$

where β_i $(i = 1 \sim 6)$ and b_j $(j = 1 \sim 3)$ are all curve-fitted constants. Substituting Eq. (15) into Eq. (14) leads to an explicit $P^*-\delta^*$ relation, which is helpful for further development.

For $\mu < 1$, we need to consider both the intimate contact and noncontact extension regimes. Under this circumstance, the $P^*-\delta^*$ relation are found to be

$$P^* = M_1 + M_2\left\{\exp\left(-\frac{(\delta^*-d_1)^2}{2d_2}\right) + M_3[1-\tanh(d_3(\delta^*-d_4))] \times \exp\left(\frac{d_5}{2}|\delta^*-d_6| + \delta^* - d_6\right)\right\} \tag{16}$$

where M_i $(i = 1 \sim 3)$ and d_j $(j = 1 \sim 6)$ are all curve-fitted parameters. Figure 4 depicts fitted-curves for different values of μ, and shows that the curve fitting results (triangles) match well with the exact solution of the double-Hertz model (lines).

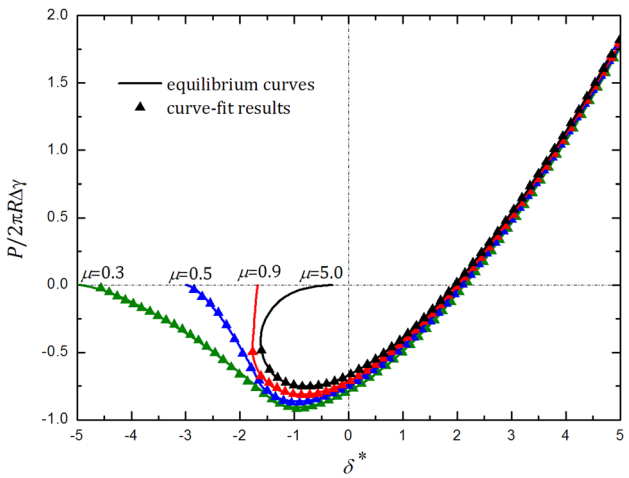

Fig. 4 Comparison between the exact double-Hertz solutions (lines) and the corresponding fitted curves (triangles)

Table 1 Curve-fitted parameters for $\mu \geq 1$

μ	β_1	β_2	β_3	β_4	β_5	β_6	b_1	b_2	b_3
1.0	−0.437	−1.020	1.957	0.293	1.676	0.961	0.678	2.590	0.499
1.2	−0.298	−0.683	1.451	0.370	1.600	0.922	0.231	2.962	0.501
2.0	−0.104	−0.775	1.397	0.584	1.322	0.791	0.208	3.008	0.520
3.0	−0.041	−0.796	1.433	0.668	1.248	0.761	0.208	3.008	0.525
4.0	−0.022	−0.799	1.457	0.700	1.225	0.753	0.209	3.006	0.526
5.0	−0.029	−0.806	1.527	0.716	1.214	0.750	0.232	2.961	0.527

The corresponding curve-fitted parameters for $\mu \geq 1$ and $\mu < 1$ are listed in Table 1 and Table 2, respectively. These approximate but explicit $P^* - \delta^*$ equations constitute the basis for the subsequent contact analysis involving rough surfaces.

4 Rough Adhesive Contact Model

In this section, we shall establish a rough adhesive contact model with use of the results developed in previous sections. A sketch of the adhesive contact between a rigid smooth surface and a randomly rough elastic surface is illustrated in Fig. 5(*a*), where the real surface roughness may be very complicated in topography. Based on the reference plane of the rough surface defined by the mean asperity height, z measures the asperity height, while d represents the distance between the contacting surfaces. Following Greenwood and Williamson [10], the randomly rough surface can be modeled as an ensemble of noninteracting asperities with identical radius of curvature R and heights following Gaussian distribution (as shown in Fig. 5(*b*)) with a probability density function

$$\phi(z) = \frac{1}{\sigma\sqrt{2\pi}} \exp\left(-\frac{z^2}{2\sigma^2}\right) \tag{17}$$

where σ is the standard deviation of asperity heights. Lower values of σ correspond to smoother surface, whereas higher values of σ represent rougher surface. It should be noted that this multiple asperity contact model applies to surfaces with large roughness, in which each individual contact is independent and the interaction between asperities can be ignored [15].

When the two surfaces are brought together by a distance of d, an asperity whose height is greater than d will come into contact with the rigid surface with a probability

$$\text{Prob}(z > d) = \int_d^\infty \phi(z)\text{d}z \tag{18}$$

where $\varphi(z)\text{d}z$ is the probability that an asperity has a height between z and $z + \text{d}z$. If there are N asperities per unit area on the rough surface, the total number of asperities contacting with the smooth plane is expected to be

$$n = N\int_d^\infty \phi(z)\text{d}z \tag{19}$$

In the loading process, when the two surfaces approach to each other, the total normal force per unit area between the surfaces is the sum of the forces exerted by all contacting asperities, that is

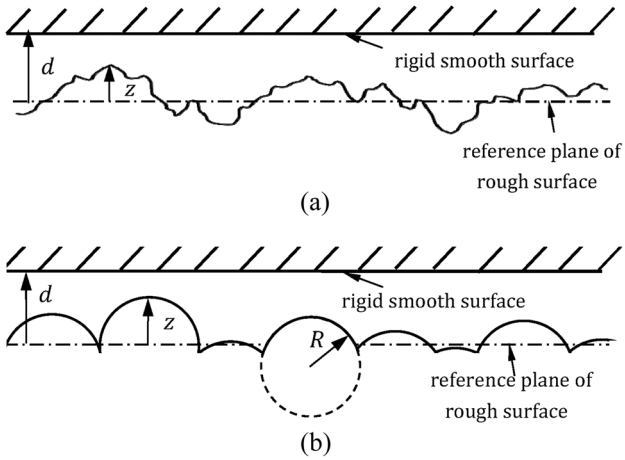

Fig. 5 Adhesive contact between a rigid smooth surface and a randomly rough elastic surface in (*a*) a real case and (*b*) a simplified model

$$P^+_{\text{rough}} = N\int_d^\infty P(\delta)\phi(z)\text{d}z = 2\pi NR\Delta\gamma\int_d^\infty P^*(\delta^*)\phi(z)\text{d}z \tag{20}$$

where $P^*(\delta^*)$ is the approximate explicit equations defined by Eqs. (14)–(15) and Eq. (16).

Since the asperities with a height greater than d are deformed by a value of $\delta = z - d$ at the tip, inserting Eq. (17) into Eq. (20) and then changing the variable of integration from z to δ give rise to the total force applied on the whole rough surface as

$$\frac{P^+_{\text{rough}}}{2\pi NR\Delta\gamma} = \frac{1}{\sigma\sqrt{2\pi}}\int_0^\infty P^*\left(\frac{\delta}{\bar{\delta}}\right)\exp\left(-\frac{(\delta+d)^2}{2\sigma^2}\right)\text{d}\delta \tag{21}$$

By introducing the normalized variables $\Delta = \delta/\sigma$, $\bar{\Delta} = \bar{\delta}/\sigma$ and $\bar{d} = d/\sigma$, Eq. (21) can be rewritten as

$$\frac{P^+_{\text{rough}}}{2N\pi R\Delta\gamma} = \frac{1}{\sqrt{2\pi}}\int_0^\infty P^*\left(\frac{\Delta}{\bar{\Delta}}\right)\exp\left(-\frac{(\Delta+\bar{d})^2}{2}\right)\text{d}\Delta \tag{22}$$

This equation determines the total forces between the two approaching surfaces during a loading stage. When the separation between the two surfaces reduces to a small enough value, the compressive force resulting from the intimate contact asperities will dominate and P^+_{rough} will then become positive from negative.

The unloading stage starts from the minimum value of d (i.e., surface separation). During the unloading stage, as the separation between the two surfaces increases, the elongation of the tips of contacting asperities (i.e., δ) will also increase gradually until reaching a critical value δ_c shown in Fig. 3. Under this condition, asperities with a height $z > d$ are in the state of compression and exert repulsive forces on the rigid surface, while those with a height $d - \delta_c < z < d$ are stretched and experience adhesive tensile forces. Consequently, the total applied force during the unloading process can be calculated as

Table 2 Curve-fitted parameters for $\mu < 1$

μ	M_1	M_2	M_3	d_1	d_2	d_3	d_4	d_5	d_6
0.2	20.533	−24.165	−0.078	−6.516	272.987	0.312	−1.839	0.206	−0.517
0.3	19.206	−20.531	−0.028	−2.823	187.880	0.769	−1.907	0.696	−0.884
0.5	7.877	−8.256	0.005	−0.579	48.524	1.708	−1.825	3.103	−2.493
0.7	9.227	−5.586	0.508	1.751	37.927	−0.610	−3.495	−0.119	−1.660
0.9	6.548	−4.417	0.664	2.379	21.355	−0.400	−2.810	−0.268	−1.663

$$\frac{P^{-}_{\text{rough}}}{2N\pi R\Delta\gamma}=\frac{1}{\sqrt{2\pi}}\int_{-\Delta_c(\mu)}^{\infty}P^{*}\left(\frac{\Delta}{\bar{\Delta}}\right)\exp\left(-\frac{(\Delta+\bar{d})^2}{2}\right)\mathrm{d}\Delta \qquad (23)$$

where $\Delta_c(\mu)=\delta_c/\sigma$ is dependent on the Tabor parameter μ.

5 The Adhesion Hysteresis and Total Pull-Off Force

As shown in Eqs. (22) and (23), the total applied forces at a given separation are different in the loading and unloading stages, which implies the existence of a adhesion hysteresis due to surface roughness. To illustrate this phenomenon more clearly, Figs. 6(*a*)–6(*b*) plot the normalized forces against the normalized separation in a loading/unloading cycle for different values of μ. It can be observed from these figures that different loading and unloading paths induced by the surface roughness compose a hysteresis loop whose area quantifies the dissipation energy during the deformation process. In fact, this hysteresis for rough surfaces can be viewed as the statistical average of the hysteresis for each individual contact asperity, which has been characterized in Fig. 3. Careful observation of Figs. 6(*a*)–6(*b*) indicates that for prescribed material properties (i.e., μ is fixed), the equilibrium curves are dependent on the surface roughness only through a dimensionless parameter $1/\bar{\Delta}$ (termed as the adhesion parameter in the following discussions). Since $1/\bar{\Delta}(=\bar{\delta}/\sigma)$ is proportional to the standard deviation σ of asperity heights for given material properties (note that $\bar{\delta}$ defined in Eq. (7) is fixed), larger $1/\bar{\Delta}$ corresponds to rougher surfaces, whereas lower $1/\bar{\Delta}$ corresponds to smoother surfaces.

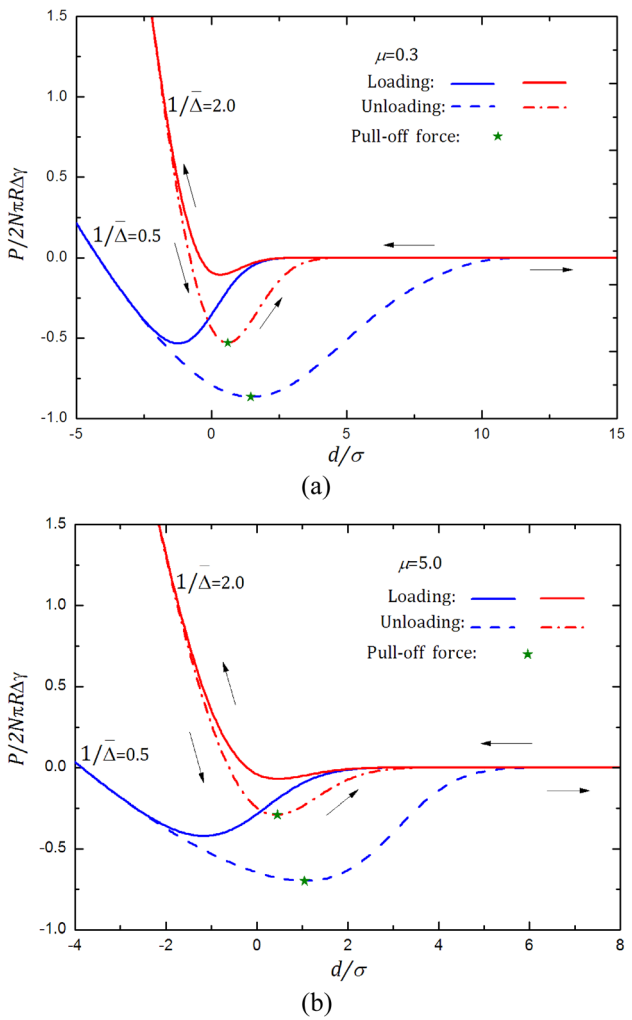

Fig. 6 The variation of normalized loading forces with respect to the normalized separation during a loading/unloading cycle for (*a*) $\mu=0.3$ and (*b*) $\mu=5$, respectively

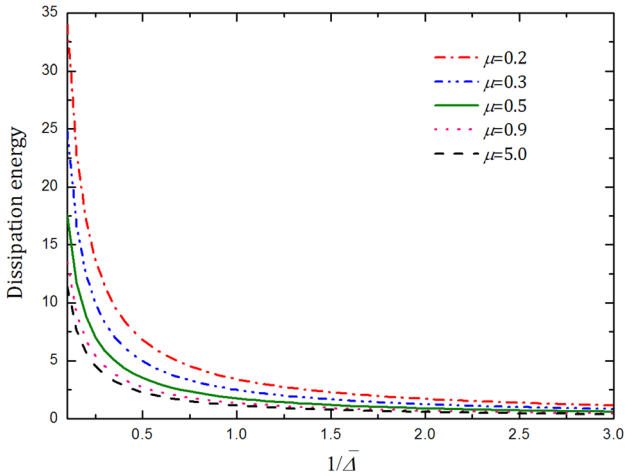

Fig. 7 Energy dissipation due to adhesion hysteresis as a function of the adhesion parameter $1/\bar{\Delta}$ in a loading/unloading cycle

Figure 7 plots the variations of the dissipation energy due to hysteresis with the dimensionless parameter $1/\bar{\Delta}$ for various values of μ. It can be seen that as the surface becomes rougher with increasing $1/\bar{\Delta}$, the dissipation energy decreases and tends to zero for all values of μ. Another observation that can be made from this figure is that the total energy loss is a function of μ. For a given surface topography ($1/\bar{\Delta}$ is fixed), the dissipation energy for soft materials corresponding to larger values of μ is smaller than that for hard materials corresponding to smaller values of μ. This phenomenon can be explained by the contact behavior of individual asperities shown in Fig. 3. Actually, when μ is small, the adhesive force will decay more slowly with larger values of δ_c, which in turn renders the corresponding energy dissipation measured by the enclosed area larger. Consequently, the total energy dissipation due to surface roughness is predicted to decrease with increasing values of μ.

On the other hand, the total pull-off force for rough adhesion, as a measure of the adhesion strength of the contact system, is quantified by the most negative value of the total applied force during the unloading process, which is shown in Figs. 6(*a*)–6(*b*). As the separation between two surfaces increases, the total force becomes tensile (negative), reaches a minimum value (pull-off force), and then tends asymptotically to zero when d is sufficient large (i.e., the adhesion between the highest asperities is broken).

Figure 8 depicts the variations of the total pull-off force against the adhesion parameter $1/\bar{\Delta}$ for different values of μ. As P_c^* represents the normalized pull-off force for an individual asperity, the vertical axis $P_{\text{pull-off}}/2N\pi R\Delta\gamma P_c^*$ corresponds to the reduction in the pull-off force due to the dispersion of the asperity heights, where $2N\pi R\Delta\gamma P_c^*$ expresses the sum of the pull-off force exerted by N asperities per unite area on the rough surface. For the special case of $1/\bar{\Delta}=0$, i.e., $\sigma=0$, the rough surface turns out to be an ensemble of spherical asperities with the same radius and height, and $2N\pi R\Delta\gamma P_c^*$ is the maximum value attainable since these asperities are assumed to deform independently of each other. As the surface becomes rougher with increasing $1/\bar{\Delta}$, the total pull-off force decreases smoothly to zero for all values of μ. Besides, for the same surface topography (i.e., $1/\bar{\Delta}$ is fixed), decreasing μ leads to increasing magnitude of the pull-off force, which is quite consistent with the case of a single contact asperity.

From the above discussions, it can be concluded that both the adhesion toughness (measured by the dissipation energy) and strength (measured by the total pull-off force) are influenced by the surface roughness through the adhesion parameter. In fact, we have

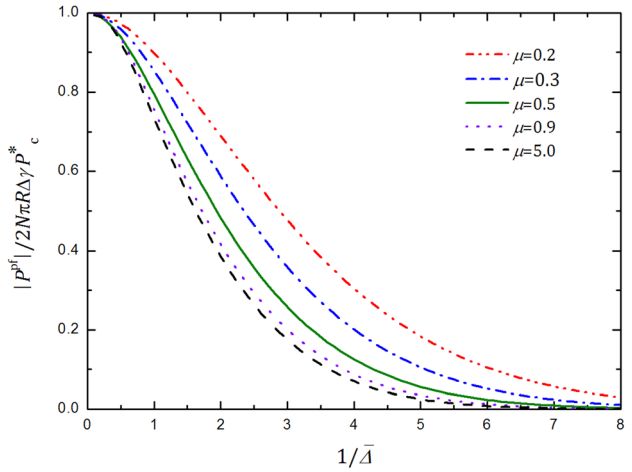

Fig. 8 Total pull-off force for rough surfaces versus the adhesion parameter $1/\bar{\Delta}$ for different values of μ

$$\frac{1}{\bar{\Delta}} = \frac{\sigma}{(R\Delta\gamma^2/E^{*2})^{1/3}} = \left(\frac{3\pi}{2}\frac{F_E}{F_A}\right)^{\frac{2}{3}} \tag{24}$$

where

$$F_E = \frac{4}{3}E^* R^{\frac{1}{2}}\sigma^{\frac{3}{2}}, \quad F_A = 2\pi R\Delta\gamma \tag{25}$$

Interestingly, F_E corresponds to elastic compressive (Hertzian) force required to press a sphere of radius R to a depth of σ into an elastic solid of modulus E^*, while F_A denotes the adhesive tensile force maintained by a sphere of radius R. The adhesion parameter can be treated as the statistical average of a competition between compressive and adhesive forces imposed by asperities with different heights, which was also found in the JKR-based rough contact model [11,35]. When $1/\bar{\Delta}$ is small, the adhesive tensile forces contributed by lower asperities win over the elastic compressive forces exerted by higher asperities. Under this circumstance, the adhesion effect of the rough surface becomes a dominant factor and hence the adhesion hysteresis and the total pull-off force turn out to be high. Both these two values reach their maximum near the limit of $1/\bar{\Delta} = 0$. On the contrary, as $1/\bar{\Delta}$ becomes larger, the elastic compressive forces exerted by higher asperities outperform the adhesive tensile forces contributed by lower asperities and therefore the effect of adhesion becomes weak. Accordingly, the corresponding adhesion hysteresis and the total pull-off force become small. For a rough surface with large enough values of $1/\bar{\Delta}$, the whole contact process occurs in the absence of adhesion and the adhesion hysteresis and the total adhesive force will vanish.

6 Conclusions

Based on the classical double-Hertz model and the multiple asperity contact model, the present paper has established an adhesive contact model for rough surfaces, which can be applied to general material properties characterized by a Tabor parameter. Our analysis results reveal that surface roughness can influence the total pull-off force and the energy dissipation resulting from loading/unloading hysteresis only through a dimensionless parameter, which measures the statistical average of a competition between compressive and adhesive forces imposed by asperities with different heights. When the adhesion parameter is small, the adhesive effect will dominate and therefore both the energy dissipation and the pull-off force will be larger. In contrast, when the adhesion parameter is relatively large, the rougher the contact surface, the smaller the adhesion effect. Under this circumstance, the corresponding energy dissipation and pull-off force will be lower. These findings may be helpful for designing and controlling the contact systems involving rough surfaces.

Acknowledgment

The financial supports from the National Natural Science Foundation (10925209, 91216201, and 10932003), 973 Project of China (2010CB832703), Program for Changjiang Scholars and Innovative Research Team in University (PCSIRT) are gratefully acknowledged.

References

[1] Johnson, K. L., Kendall, K., and Roberts, A. D., 1971, "Surface Energy and the Contact of Elastic Solids," Proc. R. Soc. Lond. A, **324**, pp. 301–313.
[2] Derjaguin, B. V., Muller, V. M., and Toporov, Y. P., 1975, "Effect of Contact Deformations on the Adhesion of Particles," J. Colloid Interface Sci., **53**, pp. 314–326.
[3] Maugis, D., 1992, "Adhesion of Spheres: The JKR-DMT Transition Using a Dugdale Model," J. Colloid Interface Sci., **150**, pp. 243–269.
[4] Tabor, D., 1977, "Surface Forces and Surface Interactions," J. Colloid Interface Sci., **58**, pp. 2–13.
[5] Shi, X., and Zhao Y. P., 2004, "Comparison of Various Adhesion Contact Theories and the Influence of Dimensionless Load Parameter," J. Adhes. Sci. Technol., **18**, pp. 55–68.
[6] Greenwood, J. A., and Johnson, K. L., 1998, "An Alternative to the Maugis Model of Adhesion Between Elastic Spheres," J. Phys. D: Appl. Phys., **31**, pp. 3279–3290.
[7] Persson, B. N. J., 2002, "Adhesion Between an Elastic Body and a Randomly Rough Hard Surface," Eur. Phys. J. E, **8**, pp. 385–401.
[8] Haiat, G., Huy, M. C. P., and Barthel, E., 2003, "The Adhesive Contact of Viscoelastic Spheres," J. Mech. Phys. Solids, **51**, pp. 69–99.
[9] Jin, F., Guo, X., and Gao, H., 2013, "Adhesive Contact on Power-Law Graded Elastic Solids: The JKR-DMT Transition Using a Double-Hertz Model," J. Mech. Phys. Solids, **61**, pp. 2473–2492.
[10] Greenwood, J. A., and Williamson, J. B. P., 1966, "Contact of Nominally Flat Surfaces," Proc. R. Soc. Lond. A, **295**, pp. 300–319.
[11] Fuller, K. N. G., and Tabor, D., 1975, "The Effect of Surface Roughness on Adhesion of Elastic Solids," Proc. R. Soc. Lond. A, **345**, pp. 327–342.
[12] Maugis, D., 2000, *Contact, Adhesion and Rupture of Elastic Solids*, Springer-Verlag, Berlin.
[13] Morrow, C., Lovell, M. R., and Ning, X., 2003, "A JKR-DMT Transition Solution for Adhesive Rough Surface Contact," J. Phy. D Appl. Phys., **36**, pp. 534–540.
[14] Kim, H. C., and Russell, T. P., 2001, "Contact of Elastic Solids With Rough Surfaces," J. Polym. Sci., Part B, **39**, pp. 1848–1854.
[15] Kesari, H., Doll, J., Pruitt, B., Wei, C., and Lew, A., 2010, "The Role of Surface Roughness During Adhesive Elastic Contact," Philos. Mag. Lett., **90**, pp. 891–902.
[16] Wang, L. F., Rong, W. B., Shao, B., and Sun, L. N., 2012, "Adhesion Elastic Contact of Rough Surface With Power-Law Axisymmetric Asperities," ASME J. Tribol., **134**(3), p. 032101.
[17] Chandrasekar, S., Eriten, M., and Polycarpou, A. A., 2012, "An Improved Model of Asperity Interaction in Normal Contact of Rough Surface," ASME J. Appl. Mech., **80**(1), p. 011025.
[18] Ciavarella, M., Greenwood, J., and Paggi, M., 2008, "Inclusion of 'Interaction' in the Greenwood and Williamson Contact Theory," Wear, **265**, pp. 729–734.
[19] Vakis, A. I., 2013, "Asperity Interaction and Substrate Deformation in Statistical Summation Models of Contact Between Rough Surfaces," ASME J. Appl. Mech., **81**(4), p. 041012.
[20] Liou, J. L., and Lin, J. F., 2008, "A Microcontact Non-Gaussian Surfaces Roughness Model Accounting for Elastic Recovery," ASME J. Appl. Mech., **75**(3), p. 031015.
[21] Eriten, M., Polycarpou, A. A., and Bergman, L. A., 2011, "Surface Roughness Effects on Energy Dissipation in Fretting Contact of Nominally Flat Surfaces," ASME J. Appl. Mech., **78**(2), p. 021011.
[22] Persson, B. N. J., and Tosatti, E., 2001, "The Effect of Surface Roughness on the Adhesion of Elastic Solids," J. Chem. Phys., **115**, pp. 5597–5610.
[23] Hui, C. Y., Lin, Y. Y., Baney, J. M., and Kramer, E. J., 2001, "The Mechanics of Contact and Adhesion of Periodically Rough Surfaces," J. Polym. Sci., B, **39**, pp. 1195–1214.
[24] Johnson, K. L., 1995, "The Adhesion of Two Elastic Bodies With Slightly Wave Surfaces," Int. J. Solids Struct., **32**, pp. 423–430.
[25] Carbone, G., and Mangialardi, L., 2004, "Adhesion and Friction of an Elastic Half-Space in Contact With a Slightly Wavy Rigid Surface," J. Mech. Phys. Solids, **52**, pp. 1267–1287.
[26] Adams, G. G., 2004, "Adhesion at the Wavy Contact Interface Between Two Elastic Bodies," ASME J. Appl. Mech., **71**(6), pp. 851–856.
[27] Guduru, P. R., 2007, "Detachment of a Rigid Solid From an Elastic Wavy Surface: Theory," J. Mech. Phys. Solids, **55**, pp. 445–472.
[28] Guduru, P. R., and Bull, C., 2007, "Detachment of a Rigid Solid From an Elastic Wavy Surface: Experiment," J. Mech. Phys. Solids, **55**, pp. 473–488.
[29] Waters, J. F., Lee, S., and Guduru, P. R., 2009, "Mechanics of Axisymmetric Wavy Surface Adhesion: JKR-DMT Transition Solution," Int. J. Solids Struct., **46**, pp. 1033–1042.

[30] Yao, H., 2013, "A Generalized Mode for Adhesive Contact Between a Rigid Cylinder and a Transversely Isotropic Substrate," ASME J. Appl. Mech., **80**(1), p. 011027.
[31] Zappone, B., Rosenberg, K., and Israelachvili, J., 2007, "Role of Nanometer Roughness on the Adhesion and Friction of a Rough Polymer Surface and a Molecularly Smooth Mica Surface," Tribol. Lett., **26**, pp. 191–201.
[32] Li, Q., and Kim, K., 2009, "Micromechanics of Rough Surface Adhesion: A Homogenized Projection Method," Acta Mech. Solida Sin., **22**, pp. 377–390.
[33] Kesari, H., and Lew, A., 2011, "Effective Macroscopic Adhesive Contact Behavior Induced by Small Surface Roughness," J. Mech. Phys. Solids, **59**, pp. 2488–2510.
[34] Jin, F., and Guo, X., 2013, "Mechanics of Axisymmetric Adhesive Contact of Rough Surfaces Involving Power-Law Graded Materials," Int. J. Solids Struct., **50**, pp. 3375–3386.
[35] Wei, Z., He, M., and Zhao, Y. P., 2010, "The Effects of Roughness on Adhesion Hysteresis," J. Adhesion Sci. Technol., **24**, pp. 1045–1054.